DESY 07-100

July 2007

Forward-jet production in deep inelastic ep scattering at HERA

ZEUS Collaboration

Abstract

Forward jet cross sections have been measured in neutral current deep inelastic scattering at low Bjorken-x with the ZEUS detector at HERA using an integrated luminosity of 81.8 pb^{-1}. Measurements are presented for inclusive forward jets as well as for forward jets accompanied by a dijet system. The explored phase space, with jet pseudorapidity up to 4.3 is expected to be particularly sensitive to the dynamics of QCD parton evolution at low x. The measurements are compared to fixed-order QCD calculations and to leading-order parton-shower Monte Carlo models.

The ZEUS Collaboration

S. Chekanov[1], M. Derrick, S. Magill, B. Musgrave, D. Nicholass[2], J. Repond, R. Yoshida
Argonne National Laboratory, Argonne, Illinois 60439-4815, USA [n]

M.C.K. Mattingly
Andrews University, Berrien Springs, Michigan 49104-0380, USA

M. Jechow, N. Pavel †, A.G. Yagües Molina
Institut für Physik der Humboldt-Universität zu Berlin, Berlin, Germany

S. Antonelli, P. Antonioli, G. Bari, M. Basile, L. Bellagamba, M. Bindi, D. Boscherini, A. Bruni, G. Bruni, L. Cifarelli, F. Cindolo, A. Contin, M. Corradi, S. De Pasquale, G. Iacobucci, A. Margotti, R. Nania, A. Polini, G. Sartorelli, A. Zichichi
University and INFN Bologna, Bologna, Italy [e]

D. Bartsch, I. Brock, H. Hartmann, E. Hilger, H.-P. Jakob, M. Jüngst, O.M. Kind[3], A.E. Nuncio-Quiroz, E. Paul[4], R. Renner[5], U. Samson, V. Schönberg, R. Shehzadi, M. Wlasenko
Physikalisches Institut der Universität Bonn, Bonn, Germany [b]

N.H. Brook, G.P. Heath, J.D. Morris
H.H. Wills Physics Laboratory, University of Bristol, Bristol, United Kingdom [m]

M. Capua, S. Fazio, A. Mastroberardino, M. Schioppa, G. Susinno, E. Tassi
Calabria University, Physics Department and INFN, Cosenza, Italy [e]

J.Y. Kim[6], K.J. Ma[7]
Chonnam National University, Kwangju, South Korea [g]

Z.A. Ibrahim, B. Kamaluddin, W.A.T. Wan Abdullah
Jabatan Fizik, Universiti Malaya, 50603 Kuala Lumpur, Malaysia [r]

Y. Ning, Z. Ren, F. Sciulli
Nevis Laboratories, Columbia University, Irvington on Hudson, New York 10027 [o]

J. Chwastowski, A. Eskreys, J. Figiel, A. Galas, M. Gil, K. Olkiewicz, P. Stopa, L. Zawiejski
The Henryk Niewodniczanski Institute of Nuclear Physics, Polish Academy of Sciences, Cracow, Poland [i]

L. Adamczyk, T. Bołd, I. Grabowska-Bołd, D. Kisielewska, J. Łukasik, M. Przybycień, L. Suszycki
Faculty of Physics and Applied Computer Science, AGH-University of Science and Technology, Cracow, Poland [p]

A. Kotański[8], W. Słomiński[9]
Department of Physics, Jagellonian University, Cracow, Poland

V. Adler[10], U. Behrens, I. Bloch, C. Blohm, A. Bonato, K. Borras, R. Ciesielski, N. Coppola, A. Dossanov, V. Drugakov, J. Fourletova, A. Geiser, D. Gladkov, P. Göttlicher[11], J. Grebenyuk, I. Gregor, T. Haas, W. Hain, C. Horn[12], A. Hüttmann, B. Kahle, I.I. Katkov, U. Klein[13], U. Kötz, H. Kowalski, E. Lobodzinska, B. Löhr, R. Mankel, I.-A. Melzer-Pellmann, S. Miglioranzi, A. Montanari, T. Namsoo, D. Notz, L. Rinaldi, P. Roloff, I. Rubinsky, R. Santamarta, U. Schneekloth, A. Spiridonov[14], H. Stadie, D. Szuba[15], J. Szuba[16], T. Theedt, G. Wolf, K. Wrona, C. Youngman, W. Zeuner
Deutsches Elektronen-Synchrotron DESY, Hamburg, Germany

W. Lohmann, S. Schlenstedt
Deutsches Elektronen-Synchrotron DESY, Zeuthen, Germany

G. Barbagli, E. Gallo, P. G. Pelfer
University and INFN Florence, Florence, Italy [e]

A. Bamberger, D. Dobur, F. Karstens, N.N. Vlasov[17]
Fakultät für Physik der Universität Freiburg i.Br., Freiburg i.Br., Germany [b]

P.J. Bussey, A.T. Doyle, W. Dunne, M. Forrest, D.H. Saxon, I.O. Skillicorn
Department of Physics and Astronomy, University of Glasgow, Glasgow, United Kingdom [m]

I. Gialas[18], K. Papageorgiu
Department of Engineering in Management and Finance, Univ. of Aegean, Greece

T. Gosau, U. Holm, R. Klanner, E. Lohrmann, H. Salehi, P. Schleper, T. Schörner-Sadenius, J. Sztuk, K. Wichmann, K. Wick
Hamburg University, Institute of Exp. Physics, Hamburg, Germany [b]

C. Foudas, C. Fry, K.R. Long, A.D. Tapper
Imperial College London, High Energy Nuclear Physics Group, London, United Kingdom [m]

M. Kataoka[19], T. Matsumoto, K. Nagano, K. Tokushuku[20], S. Yamada, Y. Yamazaki[21]
Institute of Particle and Nuclear Studies, KEK, Tsukuba, Japan [f]

A.N. Barakbaev, E.G. Boos, N.S. Pokrovskiy, B.O. Zhautykov
Institute of Physics and Technology of Ministry of Education and Science of Kazakhstan, Almaty, Kazakhstan

V. Aushev[1], M. Borodin, A. Kozulia, M. Lisovyi
Institute for Nuclear Research, National Academy of Sciences, Kiev and Kiev National University, Kiev, Ukraine

D. Son
Kyungpook National University, Center for High Energy Physics, Daegu, South Korea [g]

J. de Favereau, K. Piotrzkowski
Institut de Physique Nucléaire, Université Catholique de Louvain, Louvain-la-Neuve, Belgium [q]

F. Barreiro, C. Glasman[22], M. Jimenez, L. Labarga, J. del Peso, E. Ron, M. Soares, J. Terrón, M. Zambrana
Departamento de Física Teórica, Universidad Autónoma de Madrid, Madrid, Spain [l]

F. Corriveau, C. Liu, R. Walsh, C. Zhou
Department of Physics, McGill University, Montréal, Québec, Canada H3A 2T8 [a]

T. Tsurugai
Meiji Gakuin University, Faculty of General Education, Yokohama, Japan [f]

A. Antonov, B.A. Dolgoshein, V. Sosnovtsev, A. Stifutkin, S. Suchkov
Moscow Engineering Physics Institute, Moscow, Russia [j]

R.K. Dementiev, P.F. Ermolov, L.K. Gladilin, L.A. Khein, I.A. Korzhavina, V.A. Kuzmin, B.B. Levchenko[23], O.Yu. Lukina, A.S. Proskuryakov, L.M. Shcheglova, D.S. Zotkin, S.A. Zotkin
Moscow State University, Institute of Nuclear Physics, Moscow, Russia [k]

I. Abt, C. Büttner, A. Caldwell, D. Kollar, W.B. Schmidke, J. Sutiak
Max-Planck-Institut für Physik, München, Germany

G. Grigorescu, A. Keramidas, E. Koffeman, P. Kooijman, A. Pellegrino, H. Tiecke, M. Vázquez[19], L. Wiggers
NIKHEF and University of Amsterdam, Amsterdam, Netherlands [h]

N. Brümmer, B. Bylsma, L.S. Durkin, A. Lee, T.Y. Ling
Physics Department, Ohio State University, Columbus, Ohio 43210 [n]

P.D. Allfrey, M.A. Bell, A.M. Cooper-Sarkar, R.C.E. Devenish, J. Ferrando, B. Foster, K. Korcsak-Gorzo, K. Oliver, S. Patel, V. Roberfroid[24], A. Robertson, P.B. Straub, C. Uribe-Estrada, R. Walczak
Department of Physics, University of Oxford, Oxford United Kingdom [m]

P. Bellan, A. Bertolin, R. Brugnera, R. Carlin, F. Dal Corso, S. Dusini, A. Garfagnini, S. Limentani, A. Longhin, L. Stanco, M. Turcato
Dipartimento di Fisica dell' Università and INFN, Padova, Italy [e]

B.Y. Oh, A. Raval, J. Ukleja[25], J.J. Whitmore[26]
Department of Physics, Pennsylvania State University, University Park, Pennsylvania 16802 [o]

Y. Iga
Polytechnic University, Sagamihara, Japan [f]

G. D'Agostini, G. Marini, A. Nigro
Dipartimento di Fisica, Università 'La Sapienza' and INFN, Rome, Italy [e]

J.E. Cole, J.C. Hart
Rutherford Appleton Laboratory, Chilton, Didcot, Oxon, United Kingdom [m]

H. Abramowicz[27], A. Gabareen, R. Ingbir, S. Kananov, A. Levy
Raymond and Beverly Sackler Faculty of Exact Sciences, School of Physics, Tel-Aviv University, Tel-Aviv, Israel [d]

M. Kuze, J. Maeda
Department of Physics, Tokyo Institute of Technology, Tokyo, Japan [f]

R. Hori, S. Kagawa[28], N. Okazaki, S. Shimizu, T. Tawara
Department of Physics, University of Tokyo, Tokyo, Japan [f]

R. Hamatsu, H. Kaji[29], S. Kitamura[30], O. Ota, Y.D. Ri
Tokyo Metropolitan University, Department of Physics, Tokyo, Japan [f]

M.I. Ferrero, V. Monaco, R. Sacchi, A. Solano
Università di Torino and INFN, Torino, Italy [e]

M. Arneodo, M. Ruspa
Università del Piemonte Orientale, Novara, and INFN, Torino, Italy [e]

S. Fourletov, J.F. Martin
Department of Physics, University of Toronto, Toronto, Ontario, Canada M5S 1A7 [a]

S.K. Boutle[18], J.M. Butterworth, C. Gwenlan[31], T.W. Jones, J.H. Loizides, M.R. Sutton[31], M. Wing
Physics and Astronomy Department, University College London, London, United Kingdom [m]

B. Brzozowska, J. Ciborowski[32], G. Grzelak, P. Kulinski, P. Łużniak[33], J. Malka[33], R.J. Nowak, J.M. Pawlak, T. Tymieniecka, A. Ukleja, A.F. Żarnecki
Warsaw University, Institute of Experimental Physics, Warsaw, Poland

M. Adamus, P. Plucinski[34]
Institute for Nuclear Studies, Warsaw, Poland

Y. Eisenberg, I. Giller, D. Hochman, U. Karshon, M. Rosin
Department of Particle Physics, Weizmann Institute, Rehovot, Israel [c]

E. Brownson, T. Danielson, A. Everett, D. Kçira, D.D. Reeder[4], P. Ryan, A.A. Savin, W.H. Smith, H. Wolfe
Department of Physics, University of Wisconsin, Madison, Wisconsin 53706, USA [n]

S. Bhadra, C.D. Catterall, Y. Cui, G. Hartner, S. Menary, U. Noor, J. Standage, J. Whyte
Department of Physics, York University, Ontario, Canada M3J 1P3 [a]

[1] supported by DESY, Germany
[2] also affiliated with University College London, UK
[3] now at Humboldt University, Berlin, Germany
[4] retired
[5] self-employed
[6] supported by Chonnam National University in 2005
[7] supported by a scholarship of the World Laboratory Björn Wiik Research Project
[8] supported by the research grant no. 1 P03B 04529 (2005-2008)
[9] This work was supported in part by the Marie Curie Actions Transfer of Knowledge project COCOS (contract MTKD-CT-2004-517186)
[10] now at Univ. Libre de Bruxelles, Belgium
[11] now at DESY group FEB, Hamburg, Germany
[12] now at Stanford Linear Accelerator Center, Stanford, USA
[13] now at University of Liverpool, UK
[14] also at Institut of Theoretical and Experimental Physics, Moscow, Russia
[15] also at INP, Cracow, Poland
[16] on leave of absence from FPACS, AGH-UST, Cracow, Poland
[17] partly supported by Moscow State University, Russia
[18] also affiliated with DESY
[19] now at CERN, Geneva, Switzerland
[20] also at University of Tokyo, Japan
[21] now at Kobe University, Japan
[22] Ramón y Cajal Fellow
[23] partly supported by Russian Foundation for Basic Research grant no. 05-02-39028-NSFC-a
[24] EU Marie Curie Fellow
[25] partially supported by Warsaw University, Poland
[26] This material was based on work supported by the National Science Foundation, while working at the Foundation.
[27] also at Max Planck Institute, Munich, Germany, Alexander von Humboldt Research Award
[28] now at KEK, Tsukuba, Japan
[29] now at Nagoya University, Japan
[30] Department of Radiological Science
[31] PPARC Advanced fellow
[32] also at Łódź University, Poland
[33] Łódź University, Poland
[34] supported by the Polish Ministry for Education and Science grant no. 1 P03B 14129
[†] deceased

[a] supported by the Natural Sciences and Engineering Research Council of Canada (NSERC)

[b] supported by the German Federal Ministry for Education and Research (BMBF), under contract numbers HZ1GUA 2, HZ1GUB 0, HZ1PDA 5, HZ1VFA 5

[c] supported in part by the MINERVA Gesellschaft für Forschung GmbH, the Israel Science Foundation (grant no. 293/02-11.2) and the U.S.-Israel Binational Science Foundation

[d] supported by the German-Israeli Foundation and the Israel Science Foundation

[e] supported by the Italian National Institute for Nuclear Physics (INFN)

[f] supported by the Japanese Ministry of Education, Culture, Sports, Science and Technology (MEXT) and its grants for Scientific Research

[g] supported by the Korean Ministry of Education and Korea Science and Engineering Foundation

[h] supported by the Netherlands Foundation for Research on Matter (FOM)

[i] supported by the Polish State Committee for Scientific Research, grant no. 620/E-77/SPB/DESY/P-03/DZ 117/2003-2005 and grant no. 1P03B07427/2004-2006

[j] partially supported by the German Federal Ministry for Education and Research (BMBF)

[k] supported by RF Presidential grant N 8122.2006.2 for the leading scientific schools and by the Russian Ministry of Education and Science through its grant Research on High Energy Physics

[l] supported by the Spanish Ministry of Education and Science through funds provided by CICYT

[m] supported by the Particle Physics and Astronomy Research Council, UK

[n] supported by the US Department of Energy

[o] supported by the US National Science Foundation. Any opinion, findings and conclusions or recommendations expressed in this material are those of the authors and do not necessarily reflect the views of the National Science Foundation.

[p] supported by the Polish Ministry of Science and Higher Education as a scientific project (2006-2008)

[q] supported by FNRS and its associated funds (IISN and FRIA) and by an Inter-University Attraction Poles Programme subsidised by the Belgian Federal Science Policy Office

[r] supported by the Malaysian Ministry of Science, Technology and Innovation/Akademi Sains Malaysia grant SAGA 66-02-03-0048

1 Introduction

Deep inelastic lepton scattering (DIS) off protons provides a rich field for exploring the parton dynamics in QCD. HERA has extended the phase-space region in the Bjorken scaling variable, x_{Bj}, down to a few 10^{-5}. At such low x_{Bj}, several steps in the QCD cascade initiated by a parton from the proton can occur before the final interaction with the virtual photon takes place. The result of this cascade may be observed in the final state and provides an opportunity to study the QCD parton evolution in detail.

Within perturbative QCD (pQCD), fixed-order calculations for the parton evolution are so far available only at next-to-leading order (NLO). A number of different approximations to the QCD evolution have been developed, based on summing of particular subsets of diagrams in accordance with their importance in the phase space considered.

The conventional DGLAP [1–3] approach sums up the leading logarithms in the virtuality of the exchanged boson, Q^2, and is expected to be valid at not too small x_{Bj} and Q^2. At small x_{Bj}, a better approximation is expected to be provided by the BFKL formalism [4] which resums the leading logarithm terms in $1/x$, where x is the fractional longitudinal momentum of a parton. The CCFM [5, 6] approach interpolates between the two types of evolution, DGLAP and BFKL.

The DGLAP evolution equations have been successfully tested at HERA in inclusive measurements at low x_{Bj} and no indication of BFKL dynamics was observed. The dynamics at low x_{Bj} can be further probed by measurements of the partonic final state that highlight the differences between predictions of the BFKL and DGLAP formalisms. BFKL evolution results in a larger fraction of small x_{Bj} events with forward jets[1] than the DGLAP evolution. A forward jet is characterised by a high fractional longitudinal momentum, $x^{\mathrm{jet}} = p_Z^{\mathrm{jet}}/p$, where p is the proton momentum and $p_{\mathrm{Z}}^{\mathrm{jet}}$ is the longitudinal jet momentum [7].

A comparison of data on forward jets with the DGLAP leading-order parton-shower Monte Carlo programmes performed previously in DIS at HERA [8–10] has revealed a clear deficit of forward jets in the Monte Carlo. However, the addition of a parton cascade evolved according to DGLAP on the photon side has significantly improved the description [11]. The simulation based on the Color Dipole Model (CDM) [12–14], which includes parton emissions not ordered in transverse momentum, also succeeded in describing the data. Fixed-order NLO QCD calculations [15, 16] were also compared to the forward jets measurements in more recent publications and failed to describe the data. These studies

[1] The ZEUS coordinate system is a right-handed Cartesian system, with the Z axis pointing in the proton beam direction, referred to as the "forward direction", and the X axis pointing towards the centre of HERA. The coordinate origin is at the nominal interaction point.

were performed up to pseudorapidities 3 [17] and 2.7 [18].

In this paper, measurements of inclusive forward-jet cross sections for pseudorapidities of up to 4.3 are presented, based on a data sample which corresponds to a twofold increase in luminosity with respect to the previous ZEUS analysis [17]. Furthermore, a comparison of the measured cross sections with the CASCADE Monte Carlo [19], based on the CCFM evolution, is presented. In addition, measurements of "forward jet + dijet" cross sections, as investigated by the H1 Collaboration [18], are reported. These measurements explore parton evolution in a more exclusive way and are more sensitive to its details.

2 Theoretical framework and phase-space definitions

The DGLAP evolution equations, based on collinear factorisation, assume that the dominant contribution to parton evolution comes from subsequent parton emissions that are strongly ordered in transverse momenta, k_T, where the parton with the largest k_T interacts with the photon. In this formalism, only the leading terms in $\ln Q^2$ in the QCD perturbative expansion are summed up. Since this approximation does not resum leading $\ln 1/x$ terms, it may not be adequate at low x_{Bj}.

Contrary to the DGLAP approach, the BFKL evolution equation resums the leading $\ln 1/x$ and the evolution proceeds over x at fixed Q^2. The BFKL approach imposes no ordering in k_T but strong ordering in x, with the low-x parton interacting with the photon. At small x_{Bj}, the difference between these approaches to the QCD parton evolution is expected to be most prominent for hard partons created at the beginning of the cascade, i.e. at pseudorapidities close to the proton (forward region).

The CCFM approach is based on the idea of coherent gluon radiation, which leads to angular ordering of gluon emissions in the gluon ladder. It interpolates between the above two types of evolution, so it should be applicable over a larger phase-space region.

A phenomenological approach to parton evolution is provided by CDM [12–14]. In this model, gluons are emitted by color dipoles successively spanned between partons in the cascade. Due to independent radiation of the dipoles, the emitted gluons are not ordered in k_T and thus CDM mimics the BFKL-type evolution.

To investigate the relevance of different approaches, events with a jet in the forward region were analysed in the low-x_{Bj} region. Events were required to have at least one jet satisfying the following criteria:

- $(p_T^{\mathrm{jet}})^2 \sim Q^2$;
- $x^{\mathrm{jet}} \gg x_{\mathrm{Bj}}$,

where $p_T^{\rm jet}$ is the transverse momentum of the jet. The first condition suppresses strong ordering in the transverse momenta and decreases the probability of having a DGLAP-type evolution. The second condition enhances the phase space for the BFKL evolution.

A further event sample called "forward jet+dijet", which contains at least two hard jets in addition to the forward jet (fjet), was selected. The jets were ordered in pseudorapidity such that $\eta^{\rm jet_1} < \eta^{\rm jet_2} < \eta^{\rm fjet}$. For this sample, the pseudorapidity separation of dijets, $\Delta\eta_1 = \eta^{\rm jet_2} - \eta^{\rm jet_1}$, and the pseudorapidity difference between the forward and the second jet of the dijet, $\Delta\eta_2 = \eta^{\rm fjet} - \eta^{\rm jet_2}$, were studied.

The cross section as a function of $\Delta\eta_2$ was investigated for two intervals of $\Delta\eta_1$, $\Delta\eta_1 < 1$ and $\Delta\eta_1 > 1$. With such a choice of $\Delta\eta_1$, different dynamics of the partons in the cascade are expected to be highlighted. For $\Delta\eta_1 < 1$, small invariant masses of the dijet system are favoured and, therefore, partons with small values of x_g are produced, where x_g is the longitudinal momentum fraction carried by the gluon coupled to the hard dijet system (Fig. 1). Consequently, a large space is left for BFKL-type evolution in x from the forward jet to the dijet system. When $\Delta\eta_1$ is large, BFKL-like evolution can occur between the partons producing the dijet system.

3 Experimental set-up

The analysis was performed with the data taken with the ZEUS detector from 1998 to 2000, when HERA collided electrons or positrons[2] with energy of $E_e = 27.5\,\text{GeV}$ with protons of energy $E_p = 920\,\text{GeV}$, yielding a centre-of-mass energy of 318 GeV. The results are based on the sum of the e^-p and e^+p samples, corresponding to integrated luminosities of $16.4 \pm 0.3\,\text{pb}^{-1}$ and $65.3 \pm 1.5\,\text{pb}^{-1}$, respectively.

A detailed description of the ZEUS detector can be found elsewhere [20]. A brief outline of the components that are most relevant for this analysis is given below.

Charged particles are tracked in the central tracking detector (CTD) [21], which operates in a magnetic field of 1.43 T provided by a thin superconducting solenoid. The CTD consists of 72 cylindrical drift chamber layers, organised in nine superlayers covering the polar-angle region $15^\circ < \theta < 164^\circ$. The transverse-momentum resolution for full-length tracks is $\sigma(p_T)/p_T = 0.0058p_T \oplus 0.0065 \oplus 0.0014/p_T$, with p_T in GeV.

The high-resolution uranium–scintillator calorimeter (CAL) [22] consists of three parts: the forward (FCAL), the barrel (BCAL) and the rear (RCAL) calorimeters. Each part is subdivided transversely into towers and longitudinally into one electromagnetic section (EMC) and either one (in RCAL) or two (in BCAL and FCAL) hadronic sections

[2] Hereafter, both e^+ and e^- are referred to as electrons, unless explicitly stated otherwise.

(HAC). The smallest subdivision of the calorimeter is called a cell. The CAL energy resolutions, as measured under test-beam conditions, are $\sigma(E)/E = 0.18/\sqrt{E}$ for electrons and $\sigma(E)/E = 0.35/\sqrt{E}$ for hadrons, with E in GeV.

The luminosity was measured using the bremsstrahlung process $ep \to e\gamma p$ with the luminosity monitor [23], a lead-scintillator calorimeter placed in the HERA tunnel at $Z = -107$ m.

For the 1998-2000 running period, the forward plug calorimeter (FPC) [24] was installed in the 20×20 cm^2 beam hole of the FCAL, with a small hole of radius 3.15 cm in the center to accommodate the beam pipe. The FPC increased the forward calorimetric coverage by about 1 unit of pseudorapidity to $\eta \leq 5$. The FPC consisted of a lead–scintillator sandwich calorimeter divided longitudinally into electromagnetic and hadronic sections that were read out separately by wavelength-shifting fibers and photomultipliers. The energy resolution, as measured under test-beam conditions, was $\sigma(E)/E = 0.41/\sqrt{E} \oplus 0.062$ and $\sigma(E)/E = 0.65/\sqrt{E} \oplus 0.06$ for electrons and pions, respectively, with E in GeV.

4 Event selection and jet definition

A three-level trigger was used to select events online [20]. The neutral current DIS events were selected offline using criteria similar to those reported previously [25]. The main steps are outlined below.

The scattered electron was identified using an algorithm based on a neural network [26]. The kinematic variables Q^2, $x_{\rm Bj}$ and the inelasticity y were reconstructed using the double-angle method (DA) [27], where the hadronic final state was reconstructed using combinations of CTD tracks and energy clusters measured in the CAL to form energy-flow objects (EFOs) [28].

The following criteria were applied offline to select DIS events:

- a scattered electron with energy $E_e^{'}$ above 10 GeV, to ensure a well reconstructed electron and to suppress the background from photoproduction events, in which the scattered electron escapes undetected in the rear beampipe;
- $40 < \delta < 65$ GeV, where $\delta = \sum_i (E_i - P_{{\rm Z},i})$, where E_i and $P_{{\rm Z},i}$ are the energy and Z-component of the momentum of each EFO and the scattered electron. This cut removed events with large initial-state radiation and reduced the background from photoproduction events;
- $y_e < 0.95$, where $y_e = 1 - \frac{E_e^{'}}{2E_e}(1 - \cos\theta_e^{'})$ and $\theta_e^{'}$ is the polar angle of the electron. Along with the previous requirements, this reduces the photoproduction background to a negligible level;

- $|X| > 24$ cm or $|Y| > 12$ cm, where X and Y are the impact positions of the positron on the CAL, to avoid the low-acceptance region adjacent to the rear beampipe;
- the Z coordinate of the vertex, $Z_{\rm vtx}$, determined from CTD tracks, was required to be in the range $|Z_{\rm vtx}| < 50$ cm along the beam axis. This cut removed background events from non-ep interactions;
- $0.04 < y_{\rm DA} < 0.7$;
- $20 < Q^2_{\rm DA} < 100\,{\rm GeV}^2$;
- $0.0004 < x_{\rm DA} < 0.005$.

After this selection, the jets were identified using the k_T cluster algorithm [29] in the longitudinally invariant inclusive mode [30] applied in the Breit frame [31] on the CAL and FPC cells, excluding those belonging to the scattered electron. The reconstructed jets were then boosted back to the laboratory frame. Jet-energy corrections were applied in order to account for the energy loss in the inactive material in front of the detector. The events were required to have at least one jet satisfying the following criteria in the laboratory frame:

- the transverse energy of each jet was required to be $E_T^{\rm jet} > 5$ GeV;
- the pseudorapidity of each jet was required to be in the interval $2 < \eta^{\rm jet} < 4.3$;
- $x^{\rm jet} > 0.036$, which selects forward jets with large energy;
- $0.5 < (E_T^{\rm jet})^2/Q^2 < 2$, which suppresses the DGLAP-type evolution;
- jets with $2.8 < \eta^{\rm jet} < 3.35$ and with the azimuthal angle of the jet, ϕ expressed in radians, in the ranges $0 < \phi^{\rm jet} < 0.4$, $1.0 < \phi^{\rm jet} < 2.2$, $2.7 < \phi^{\rm jet} < 3.6$, $4.2 < \phi^{\rm jet} < 5.3$ or $5.7 < \phi^{\rm jet} < 6.3$ were rejected due to poor reconstruction caused by the large cell size in the FCAL;

Using the sample described above, the triple differential cross sections, with the $0.5 < (E_T^{\rm jet})^2/Q^2 < 2$ cut removed, were measured in two intervals of Q^2, $20 < Q^2 < 40$ GeV^2 and $40 < Q^2 < 100$ GeV^2 and for $E_T^{\rm jet} > 5$ GeV.

For the "forward jet+dijet" analysis, the events were required to have one forward jet, satisfying the same selection criteria as above, with the exception of the $(E_T^{\rm jet})^2/Q^2$ cut, and at least two additional jets with $E_T^{\rm jet} > 5$ GeV. The two additional jets, chosen with the highest transverse energy were required to lie in the pseudorapidity region $-1.5 < \eta^{\rm jet} < 4.3$. The three selected jets were ordered in $\eta^{\rm jet}$ as described in Section 2.

5 Monte Carlo simulations

Various MC samples were generated. Samples of LEPTO and ARIADNE generators were used to simulate the detector response to jets of hadrons and to determine the hadronisation corrections needed for comparison with perturbative QCD calculations. The same samples were used to compare the measurements to the LEPTO and ARIADNE models. In addition, the data were compared to expectations of the ARIADNE generator with its newly tuned proton-remnant treatment, "ARIADNE tuned", and to the CASCADE generator.

The LEPTO [32] MC program is based on first-order QCD matrix elements supplemented with parton showers (MEPS), which follow DGLAP evolution.

The CDM approach is represented by the ARIADNE 4.08 [33] MC program and its tuned variant ("ARIADNE tuned"[3]) as described in a recent H1 publication [18].

The CASCADE MC program [19, 34] is based on the CCFM evolution and uses k_T-factorisation of the cross section into an off-shell matrix element and an unintegrated parton (gluon) density function (uPDF). Predictions of CASCADE were obtained with the J2003 set-1 and set-2 uPDFs [35]. The J2003 set-2 includes non-singular terms in the splitting function and reduces the cross sections at low x_{Bj}.

In all MC models, the fragmentation of the final-state partons has been performed using the LUND [36] string model as implemented in JETSET 7.4 [37].

Both LEPTO and ARIADNE were interfaced to HERACLES 4.6.1 [38] via DJANGOH 1.1 [39]. The HERACLES program simulates first-order electroweak radiative corrections. The CTEQ5L [40] proton parton distribution functions (PDF) were used in both cases.

The events generated with LEPTO and ARIADNE were passed through the GEANT 3.13-based [41] ZEUS detector and trigger simulation programs [20]. They were reconstructed and analysed using the same program chain as the data.

6 Acceptance correction and systematic studies

The correction factors to the data for detector-acceptance effects were obtained with the ARIADNE and LEPTO MC programs. These correction factors were calculated bin by bin

[3] The following parameters have been changed from their default values: the powers, defining the fraction of the proton remnant participating in the emission, PARA(10)=1.2 (default=1.0) and PARA(25)=1.2 (default=2.0); the square root of the mean value of the primordial $p_\perp^2$ in the proton remnant, PARA(27)=0.9 (default=0.6).

as

$$C_{\rm Acc} = \frac{N_{\rm MC}^{\rm det}}{N_{\rm MC}^{\rm had}},$$

where $N_{\rm MC}^{\rm det}$ ($N_{\rm MC}^{\rm had}$) is the number of jets in bins of the detector (hadron) level distribution. For this approach to be valid, the distributions in the data must be well described by the MC simulation at the detector level, a condition which was in general satisfied by both ARIADNE and LEPTO. The average between the correction factors obtained with ARIADNE and LEPTO was taken. The values of $C_{\rm Acc}$ were generally between 0.4 and 1.2 for the inclusive forward-jet sample, and 0.5 to 1.4 for the "forward jet+dijet" sample.

To ensure the correct MC reconstruction of the jets near the boundary between FCAL and FPC, jet profiles in the data and MC were compared and found to be in good agreement.

The major sources of systematic uncertainty were as follows (the effects on the cross sections are shown in parentheses):

- the largest uncertainty resulted from the model dependence of the acceptance corrections. This uncertainty was estimated using the deviations of LEPTO and ARIADNE corrections from their average ($\leq$ 10% for inclusive forward jet sample, $<$ 25 % for forward jet+dijet sample);
- $\pm$ 3% shift of jet energies due to the CAL energy-scale uncertainty ($<$ 10 %);
- $\pm$ 10% shift of jet energies due to the FPC energy-scale uncertainty ($\sim$ 15% for the last $\eta^{\rm jet}$ bin, negligible elsewhere);
- the selection of inclusive DIS events ($<$ 1%). The cuts on the scattered-electron energy, the X and Y position of the electron, δ and $Z_{\rm vtx}$ were varied.

These systematic uncertainties, except for the energy-scale uncertainty, were added in quadrature separately for the positive and negative variations in each bin. The energy scale uncertainties, which are correlated between bins, are shown separately. The uncertainty in the luminosity of $\pm$ 2.2% is not included in the figures.

7 NLO QCD calculations

For inclusive forward jets, fixed-order calculations were performed with the DISENT [15] code, at $\mathcal{O}(\alpha\alpha_s^2)$ in the $\overline{\rm MS}$ renormalisation and factorisation schemes. The number of flavours was set to five; the renormalisation ($\mu_{\rm R}$) and factorisation ($\mu_{\rm F}$) scales were both set to $\mu_{\rm R} = \mu_{\rm F} = Q$. The CTEQ6M [42] parameterisation of the proton PDFs was used. The theoretical uncertainty in the calculations was estimated considering the following three sources:

- $\mu_{\rm R}$ was varied up and down by a factor of two, which contributed up to 57% depending on the phase-space region;
- $\mu_{\rm F}$ was also varied up and down by a factor of two and the resulting uncertainty was less than 5% except in the lowest $x_{\rm Bj}$ bin and the most forward region;
- the PDF uncertainty was estimated using the 40 different sets of CTEQ6 parton distribution functions [42].

For "forward jet+dijet" cross sections, the program NLOJET++ [16] was used. This program calculates three-jet production in DIS at NLO $\mathcal{O}(\alpha\alpha_s^3)$ and uses the $\overline{\rm MS}$ scheme. The number of flavours, $\mu_{\rm R}$ and $\mu_{\rm F}$ were set as in DISENT.

In order to compare the data to NLO calculations, corrections from the parton to the hadron level, C_{HAD}, were determined in each bin. The hadronisation corrections C_{HAD} were calculated as an average between those obtained from LEPTO and from ARIADNE and applied to the NLO calculations. The uncertainty of the hadronisation correction C_{HAD} was assumed to be the absolute difference in the two values.

8 Results

Cross sections for inclusive forward jets and for events containing a dijet system in addition to the forward jet, were measured in the kinematic region given by $20 < Q^2 < 100\,{\rm GeV}^2$, $0.04 < y < 0.7$ and $0.0004 < x_{\rm Bj} < 0.005$. The differential jet cross sections are presented as functions of the variable $\xi = Q^2, x_{\rm Bj}, E_T^{\rm jet}, \eta^{\rm jet}$. They were determined as

$$\frac{d\sigma}{d\xi} = \frac{N_{\rm data}^{\rm jet}}{\mathcal{L}\cdot\Delta\xi}\cdot\frac{C^{\rm QED}}{C_{\rm Acc}},$$

where $N_{\rm data}^{\rm jet}$ is the number of jets in a bin of width $\Delta\xi$, $\mathcal{L}$ is the integrated luminosity, and $C^{\rm QED} = N_{\rm MC}^{\rm noQED}/N_{\rm MC}^{\rm QED}$, where $N_{\rm MC}^{\rm QED}$ ($N_{\rm MC}^{\rm noQED}$) is the number of events selected at the hadron level in a given ξ bin in the MC sample generated with (without) QED radiation.

The triple differential cross sections were obtained in a similar manner,

$$\frac{d^3\sigma}{dQ^2 d(E_T^{\rm jet})^2 d\eta} = \frac{N_{\rm data}^{\rm jet}}{\mathcal{L}\cdot\Delta Q^2\cdot\Delta(E_T^{\rm jet})^2\cdot\Delta\eta}\cdot\frac{C^{\rm QED}}{C_{\rm Acc}}.$$

8.1 Inclusive forward-jet measurements

The measured differential forward-jet cross sections as functions of Q^2, $x_{\rm Bj}$, $E_T^{\rm jet}$ and $\eta^{\rm jet}$ are shown in Fig. 2, where they are compared to NLO calculations.

The calculations predict lower cross sections than obtained from the data by as much as a factor two; however, they have a large theoretical uncertainty. The strong dependence of the calculation on $\mu_{\rm R}$ can be related to the fact that in this kinematic region higher-order terms become relevant. As a demonstration, the leading-order calculation is also shown in Fig. 2 for each differential cross section. It is far below the measurement, indicating that the contribution of $\mathcal{O}(\alpha_{\rm s}^2)$ terms is significant. A recent publication [18], which used a harder renormalisation scale (the average E_T^2 of the dijets coming from the hard scattering), reported a smaller renormalisation-scale uncertainty.

A comparison of the data with the ARIADNE and LEPTO MC is shown in Fig. 3. The predictions of the CDM obtained with "ARIADNE default" are in fair agreement with the data with the exception of high $E_T^{\rm jet}$ and high $\eta^{\rm jet}$, where ARIADNE overestimates the cross sections. An investigation has shown that in ARIADNE the proton-remnant fragments are generated with high p_T, therefore they show up at much lower η than in other generators. The newly tuned ARIADNE, also shown in Fig. 3, yields lower cross sections, in particular at high $E_T^{\rm jet}$ and high $\eta^{\rm jet}$, and provides a good description of the data.

The predictions of the LEPTO MC are found to be in agreement with data in shape for all distributions, however the absolute normalisation is below the measurements by a factor of two.

The measurement of differential forward-jet cross sections is compared to the prediction of the CASCADE MC model in Fig. 4. Neither of the investigated uPDF sets gives a satisfactory agreement with the measurements in all distributions, suggesting that a further adjustment of the input parameters of the CASCADE model is necessary.

8.2 Triple-differential forward-jet cross section

The triple-differential forward-jet cross sections as a function of $\eta^{\rm jet}$ are presented in two intervals of Q^2 and three intervals of $(E_T^{\rm jet})^2$ in Fig. 5. Also shown in Fig. 5 are the expectations of the NLO calculations from DISENT. The calculations generally underestimate the cross sections. The largest discrepancy between the data and the theory is seen in the high-Q^2 range and for $(E_T^{\rm jet})^2 < 100$ GeV^2. This region is sensitive to multigluon emission, which is lacking in the NLO calculations.

In Fig. 6, the data are compared with LEPTO and ARIADNE. As was already observed in Fig. 3, the LEPTO MC is always below the measurements.

The cross sections of "ARIADNE tuned" are below those of the "ARIADNE default" in all the presented phase space. The difference between the two versions is smallest in the lowest-$(E_T^{\rm jet})^2$ interval, where both are close to the data. In the highest-$(E_T^{\rm jet})^2$ interval, the difference is big and "ARIADNE tuned" gives a good description of the data.

A comparison of the data with the CASCADE MC with two sets of uPDFs is shown in Fig. 7.

The expectations of CASCADE are close to the data in the low-Q^2 interval for set-1, while in the high-Q^2 interval the set-2 gives a better description of the data. None of the sets can accomodate all the features of the data.

8.3 Forward jet+dijet measurements

The measured cross sections for events with a dijet system in addition to the forward jet are compared with fixed-order QCD calculations and LO parton-shower MC models in Figs. 8-10. The cross sections are presented as a function of $\Delta\eta_1$ and $\Delta\eta_2$, and as a function of $\Delta\eta_2$ for two cases, namely, $\Delta\eta_1 < 1$ and $\Delta\eta_1 > 1$.

A comparison between data and the predictions of NLOJET++ is shown in Fig. 8. As already observed by the H1 experiment [18], the NLOJET++ calculations agree well with the data at large $\Delta\eta_2$, while they do not describe the data at small $\Delta\eta_2$, especially for small $\Delta\eta_1$. The large $\Delta\eta_2$ kinematics at low x_{Bj} favours dijets originating from photon-gluon fusion, with an additional gluon responsible for the forward jet. This case is well treated by NLOJET++. The small $\Delta\eta_1$ and $\Delta\eta_2$ region corresponds to the event configuration in which all the three jets tend to go forward, away from the hard interaction. This configuration favours multigluon emission, which is not expected to be described by NLOJET++.

The comparison between data and the LEPTO and ARIADNE MCs is shown in Fig. 9. As before, the LEPTO predictions are below the data for all differential cross sections. The "ARIADNE default" overestimates the cross sections. This implies that energetic multiple jets are produced too often in the "ARIADNE default". The tuning of the ARIADNE parameters brings this model into very good agreement with data for all differential distributions.

The comparison of the CASCADE MC to the data is presented in Fig. 10. As before, CASCADE does not satisfactorily reproduce the measurement.

9 Summary

A new measurement of the inclusive jet cross sections has been performed in an extended forward region, $2 < \eta^{\mathrm{jet}} < 4.3$, with higher statistics and smaller systematic uncertainties compared to previous studies. The measured differential cross sections are presented as functions of Q^2, x_{Bj}, E_T^{jet} and η^{jet}. The measurements were compared to the predictions of

next-to-leading-order QCD calculations, which were found to be below the data, in certain regions by as much as a factor of two. The large contribution of next-to-leading-order corrections and the size of the theoretical uncertainty indicate that in this phase space higher-order contributions are important. The best overall description of the inclusive forward-jet cross sections was obtained by the newly tuned ARIADNE MC model. The CASCADE MC with J2003 set-1 and J2003 set-2 for unintegrated gluon density failed to satisfactorily describe the data. Therefore, these measurements can be used for further adjusting the input parameters of the CASCADE model.

The measurement of the cross sections of the events containing a dijet system in addition to the forward jet is presented as functions of pseudorapidity separation between jets composing the dijet, $\Delta\eta_1$, and pseudorapidity separation between forward jet and dijet system, $\Delta\eta_2$, for all $\Delta\eta_1$ values and for $\Delta\eta_1 < 1$ and $\Delta\eta_1 > 1$. NLO calculations describe the data at large $\Delta\eta_2$ but underestimate the cross sections at small $\Delta\eta_2$, especially for small values of $\Delta\eta_1$, where, in the case of small x_{Bj}, the contribution of multiple gluon emission is expected to be large. The predictions of LEPTO are significantly below the data. ARIADNE with default parameters significantly overestimates the cross sections whereas the new tuning provides a good description of the data. The CASCADE MC, as in the inclusive case, does not provide a satisfactory description of measured cross sections.

Acknowledgments

We thank the DESY Directorate for the strong support and encouragement. We are grateful for the support of the DESY computing and network services. The diligent efforts of the HERA machine group are gratefully acknowledged. The design, construction and installation of the ZEUS detector have been made possible due to the ingenuity and efforts of many people from DESY and other institutes who are not listed as authors. We also thank Hannes Jung and Herman Hessling for fruitful discussions.

References

[1] V.N. Gribov and L.N. Lipatov, Sov. J. Nucl. Phys. **15**, 438 (1972).

[2] Yu.L. Dokshitzer, Sov. Phys. JETP **46**, 641 (1977).

[3] G. Altarelli and G. Parisi, Nucl. Phys. **B 126**, 298 (1977).

[4] Ya.Ya. Balitskiĭ and L.N. Lipatov, Sov. J. Nucl. Phys. **28**, 822 (1978).

[5] M. Ciafaloni, Nucl. Phys. **B 296**, 49 (1988).

[6] S. Catani, F. Fiorani and G. Marchesini, Nucl. Phys. **B 336**, 18 (1990).

[7] A.H. Mueller, Nucl. Phys. Proc. Suppl. **18 C**, 125 (1991).

[8] ZEUS Coll., J. Breitweg et al., Eur. Phys. J. **C 6**, 239 (1999).

[9] ZEUS Coll., J. Breitweg et al., Phys. Lett. **B 474**, 223 (2000).

[10] H1 Coll., C. Adloff et al., Nucl. Phys. **B 538**, 3 (1999).

[11] H. Jung, Comp. Phys. Comm. **86**, 147 (1995).

[12] G. Gustafson, Phys. Lett. **B 175**, 453 (1986).

[13] G. Gustafson and U. Petterson, Nucl. Phys. **B 306**, 746 (1988).

[14] B. Andersson et al., Z. Phys. **C 43**, 625 (1989).

[15] S. Catani and M.H. Seymour, Nucl. Phys. **B 485**, 579 (1998).

[16] Z. Nagy and Z. Trocsanyi, Phys. Rev. Lett. **87**, 082001 (2001).

[17] ZEUS Coll., S. Chekanov et al., Phys. Lett. **B 632**, 13 (2006).

[18] H1 Coll., A. Aktas et al., Eur. Phys. J. **C 46**, 27 (2006).

[19] H. Jung and G. P. Salam, Eur. Phys. J. **C 19** (2001).

[20] ZEUS Coll., U. Holm (ed.), *The ZEUS Detector*. Status Report (unpublished), DESY (1993), available on `http://www-zeus.desy.de/bluebook/bluebook.html`.

[21] N. Harnew et al., Nucl. Inst. Meth. **A 279**, 290 (1989);
B. Foster et al., Nucl. Phys. Proc. Suppl. **B 32**, 181 (1993);
B. Foster et al., Nucl. Inst. Meth. **A 338**, 254 (1994).

[22] M. Derrick et al., Nucl. Inst. Meth. **A 309**, 77 (1991);
A. Andresen et al., Nucl. Inst. Meth. **A 309**, 101 (1991);
A. Caldwell et al., Nucl. Inst. Meth. **A 321**, 356 (1992);
A. Bernstein et al., Nucl. Inst. Meth. **A 336**, 23 (1993).

[23] J. Andruszków et al., Preprint DESY-92-066, DESY, 1992;
ZEUS Coll., M. Derrick et al., Z. Phys. **C 63**, 391 (1994);
J. Andruszków et al., Acta Phys. Pol. **B 32**, 2025 (2001).

[24] A. Bamberger et al., Nucl. Inst. Meth. **A 450**, 235 (2000).

[25] ZEUS Coll., S. Chekanov et al., Phys. Lett. **B547**, 164 (2002).

[26] H. Abramowicz, A. Caldwell and R. Sinkus, Nucl. Inst. Meth. **A 365**, 508 (1995); R. Sinkus and T. Voss, Nucl. Inst. Meth. **A 391**, 360 (1997).

[27] S. Bentvelsen, J. Engelen and P. Kooijman, *Proc. Workshop on Physics at HERA*, W. Buchmüller and G. Ingelman (eds.), Vol. 1, p. 23. Hamburg, Germany, DESY (1992);
K.C. Höger, *Proc. Workshop on Physics at HERA*, W. Buchmüller and G. Ingelman (eds.), Vol. 1, p. 43. Hamburg, Germany, DESY (1992).

[28] ZEUS Coll., J. Breitweg et al., Eur. Phys. J. **C 1**, 81 (1998).

[29] S. Catani et al., Nucl. Phys. **B 406**, 187 (1993).

[30] S.D. Ellis and D.E. Soper, Phys. Rev. **D 48**, 3160 (1993).

[31] K.H. Streng, T.F. Walsh, P.M. Zerwas, Z. Phys. **C 2**, 237 (1979).

[32] G. Ingelman, A. Edin and J. Rathsman, Comp. Phys. Comm. **101**, 108 (1997).

[33] L. Lönnblad, Comp. Phys. Comm. **71**, 15 (1992).

[34] H. Jung, Comp. Phys. Comm. **143**, 100 (2002).

[35] H. Jung, *Strbske Pleso 2004, Deep inelastic scattering*, D. Bruncko et al. (ed.), Vol. 1, pp. 299–302. Institute of Experimental Physics SAS, Kosiće (2004). Also in preprint hep-ph/0411287.

[36] B. Andersson et al., Phys. Rep. **97**, 31 (1983).

[37] T. Sjöstrand, Comp. Phys. Comm. **82**, 74 (1994).

[38] A. Kwiatkowski, H. Spiesberger and H.-J. Möhring, Comp. Phys. Comm. **69**, 155 (1992).

[39] K. Charchula, G.A. Schuler and H. Spiesberger, Comp. Phys. Comm. **81**, 381 (1994).

[40] H.L. Lai et al., Phys. Rev. **D 55**, 1280 (1997).

[41] R. Brun et al., GEANT3, Technical Report CERN-DD/EE/84-1, CERN, 1987.

[42] J. Pumplin et al., JHEP **0602**, 032 (2006).

Q^2 bin (GeV^2)	$d\sigma/dQ^2$ ($\mathrm{pb/GeV}^2$)	δ_{stat}	δ_{syst}	δ_{CAL}	δ_{FPC}	C_{QED}	C_{HAD}
20 - 30	23.21	± 0.43	$^{+0.81}_{-0.79}$	$^{+1.39}_{-1.95}$	$^{+3.06}_{-3.03}$	0.97	0.89
30 - 40	15.49	± 0.33	$^{+0.48}_{-0.54}$	$^{+0.95}_{-1.05}$	$^{+1.73}_{-1.61}$	0.96	0.89
40 - 50	9.76	± 0.26	$^{+0.26}_{-0.37}$	$^{+0.54}_{-0.77}$	$^{+0.91}_{-1.07}$	0.94	0.89
50 - 60	6.65	± 0.21	$^{+0.27}_{-0.22}$	$^{+0.40}_{-0.36}$	$^{+0.55}_{-0.51}$	0.97	0.91
60 - 80	3.21	± 0.10	$^{+0.12}_{-0.08}$	$^{+0.20}_{-0.18}$	$^{+0.22}_{-0.22}$	0.97	0.89
80 - 100	1.36	± 0.07	$^{+0.07}_{-0.03}$	$^{+0.06}_{-0.08}$	$^{+0.08}_{-0.09}$	0.94	0.91

Table 1: *The differential cross section, $d\sigma/dQ^2$, in bins of Q^2 for inclusive forward jets. The statistical (δ_{stat}), systematic (δ_{syst}) and jet-energy-scale uncertainties for CAL and FPC (δ_{CAL} and δ_{FPC}) are shown separately. The multiplicative correction applied to correct for QED radiative effects (C_{QED}) and for hadronisation effects (C_{HAD}) are shown in the last two columns.*

x_{Bj} bin	$d\sigma/dx_{\mathrm{Bj}}$ (nb)	δ_{stat}	δ_{syst}	δ_{CAL}	δ_{FPC}	C_{QED}	C_{HAD}
0.0004 - 0.001	275	± 6	$^{+19}_{-19}$	$^{+16}_{-20}$	$^{+34}_{-35}$	0.97	0.86
0.001 - 0.002	200	± 4	$^{+10}_{-9}$	$^{+14}_{-14}$	$^{+23}_{-20}$	0.97	0.88
0.002 - 0.003	125	± 3	$^{+2}_{-3}$	$^{+6}_{-9}$	$^{+11}_{-12}$	0.96	0.90
0.003 - 0.004	89	± 2	$^{+4}_{-3}$	$^{+5}_{-6}$	$^{+9}_{-9}$	0.95	0.92
0.004 - 0.005	65	± 2	$^{+1}_{-1}$	$^{+4}_{-5}$	$^{+6}_{-6}$	0.94	0.95

Table 2: *The differential cross section, $d\sigma/dx_{\mathrm{Bj}}$, in bins of x_{Bj} for inclusive forward jets. The statistical, systematic and jet-energy-scale uncertainties are shown separately (see the caption of Table 1).*

$E_{\mathrm{T}}^{\mathrm{jet}}$ bin (GeV)	$d\sigma/dE_{\mathrm{T}}^{\mathrm{jet}}$ (pb/GeV)	δ_{stat}	δ_{syst}	δ_{CAL}	δ_{FPC}	C_{QED}	C_{HAD}
5 - 6.5	245.1	± 3.2	$^{+6.9}_{-7.6}$	$^{+15.0}_{-18.7}$	$^{+32.6}_{-31.3}$	0.96	0.91
6.5 - 8	123.2	± 2.4	$^{+4.5}_{-4.5}$	$^{+7.7}_{-8.1}$	$^{+10.0}_{-10.2}$	0.97	0.92
8 - 9.5	42.04	± 1.40	$^{+1.22}_{-1.20}$	$^{+1.9}_{-2.35}$	$^{+1.50}_{-1.69}$	0.96	0.89
9.5 - 11	13.38	± 0.73	$^{+1.17}_{-0.99}$	$^{+0.63}_{-1.49}$	$^{+0.62}_{-1.35}$	0.96	0.87
11 - 14	2.21	± 0.21	$^{+0.16}_{-0.20}$	$^{+0.05}_{-0}$	$^{+0.08}_{-0.21}$	0.93	0.89

Table 3: *The differential cross section, $d\sigma/dE_T^{\mathrm{jet}}$, in bins of E_T^{jet} for inclusive forward jets. The statistical, systematic and jet-energy-scale uncertainties are shown separately (see the caption of Table 1).*

$\eta^{\rm jet}$ bin	$d\sigma/d\eta^{\rm jet}$ (pb)	δ_{stat}	δ_{syst}	δ_{CAL}	δ_{FPC}	C_{QED}	C_{HAD}
2 - 2.3	118.0	$\pm$5.1	$^{+7.8}_{-7.8}$	$^{+8.4}_{-6.8}$	$^{+0}_{-0.1}$	0.97	0.87
2.3 - 2.6	361.4	$\pm$8.5	$^{+20.0}_{-21.0}$	$^{+24.2}_{-34.1}$	$^{+0}_{-1.3}$	0.95	0.90
2.6 - 2.9	438.2	$\pm$9.6	$^{+14.9}_{-12.4}$	$^{+40.9}_{-48.7}$	$^{+0.8}_{-1.0}$	0.96	0.93
2.9 - 3.5	331.0	$\pm$8.1	$^{+19.2}_{-20.2}$	$^{+17.0}_{-25.2}$	$^{+15.5}_{-15.4}$	0.95	0.92
3.5 - 4.3	211.6	$\pm$4.2	$^{+6.6}_{-7.7}$	$^{+4.8}_{-5.1}$	$^{+54.9}_{-79.1}$	0.98	1.01

Table 4: *The differential cross section, $d\sigma/d\eta^{\rm jet}$, in bins of $\eta^{\rm jet}$ for inclusive forward jets. The statistical, systematic and jet-energy-scale uncertainties are shown separately (see the caption of Table 1).*

$\Delta\eta_1$ bin	$d\sigma/d\Delta\eta_1$ (pb)	δ_{stat}	δ_{syst}	δ_{CAL}	δ_{FPC}	C_{QED}	C_{HAD}
0.0 - 0.7	82.88	$\pm$3.77	$^{+12.88}_{-12.88}$	$^{+8.24}_{-10.9}$	$^{+4.24}_{-4.24}$	0.98	0.74
0.7 - 1.4	79.35	$\pm$3.65	$^{+11.18}_{-11.01}$	$^{+9.40}_{-8.66}$	$^{+5.18}_{-4.13}$	0.99	0.76
1.4 - 2.1	50.68	$\pm$2.62	$^{+5.53}_{-6.12}$	$^{+4.79}_{-6.91}$	$^{+3.68}_{-3.49}$	0.98	0.76
2.2 - 4	15.30	$\pm$0.99	$^{+2.35}_{-1.67}$	$^{+1.16}_{-2.42}$	$^{+1.36}_{-2.10}$	0.96	0.75

Table 5: *The differential cross section, $d\sigma/d\Delta\eta_1$, in bins of $\Delta\eta_1$ for "forward jet+dijet" events. The statistical, systematic and jet-energy-scale uncertainties are shown separately (see the caption of Table 1).*

$\Delta\eta_2$ bin	$d\sigma/d\Delta\eta_1$ (pb)	δ_{stat}	δ_{syst}	δ_{CAL}	δ_{FPC}	C_{QED}	C_{HAD}
0.0 - 0.8	56.38	$\pm$2.64	$^{+5.26}_{-4.72}$	$^{+5.42}_{-5.97}$	$^{+1.35}_{-1.42}$	0.98	0.78
0.8 - 1.6	76.23	$\pm$3.33	$^{+5.23}_{-6.18}$	$^{+7.44}_{-9.52}$	$^{+2.51}_{-3.09}$	0.96	0.79
1.6 - 2.4	56.06	$\pm$2.82	$^{+9.33}_{-8.69}$	$^{+5.18}_{-7.31}$	$^{+4.44}_{-4.79}$	1.01	0.75
2.4 - 3.2	19.44	$\pm$1.27	$^{+4.46}_{-3.98}$	$^{+2.12}_{-2.70}$	$^{+2.69}_{-2.58}$	0.97	0.69

Table 6: *The differential cross section, $d\sigma/d\Delta\eta_2$, in bins of $\Delta\eta_2$ for "forward jet+dijet" events. The statistical, systematic and jet-energy-scale uncertainties are shown separately (see the caption of Table 1).*

$\Delta\eta_2$ bin	$d\sigma/d\Delta\eta_1$ (pb)	δ_{stat}	δ_{syst}	δ_{CAL}	δ_{FPC}	C_{QED}	C_{HAD}
0.0 - 0.8	14.86	± 1.36	$^{+1.17}_{-1.71}$	$^{+1.65}_{-1.86}$	$^{+0}_{-0.24}$	1.00	0.82
0.8 - 1.6	30.04	± 2.17	$^{+4.58}_{-5.04}$	$^{+3.21}_{-3.04}$	$^{+0.26}_{-0.34}$	0.99	0.81
1.6 - 2.4	29.48	± 1.93	$^{+4.13}_{-3.78}$	$^{+2.64}_{-3.42}$	$^{+1.12}_{-0.79}$	1.02	0.78
2.4 - 3.4	12.33	± 0.94	$^{+2.59}_{-2.27}$	$^{+1.44}_{-1.78}$	$^{+1.63}_{-1.50}$	0.96	0.68

Table 7: *The differential cross section, $d\sigma/d\Delta\eta_2$, in bins of $\Delta\eta_2$ for "forward jet+dijet" events in the case of $\Delta\eta_1 < 1$. The statistical, systematic and jet-energy-scale uncertainties are shown separately (see the caption of Table 1).*

$\Delta\eta_2$ bin	$d\sigma/d\Delta\eta_1$ (pb)	δ_{stat}	δ_{syst}	δ_{CAL}	δ_{FPC}	C_{QED}	C_{HAD}
0.0 - 0.6	40.03	± 2.28	$^{+5.32}_{-4.81}$	$^{+3.62}_{-4.12}$	$^{+1.19}_{-1.14}$	0.97	0.75
0.6 - 1.2	46.58	± 2.59	$^{+1.66}_{-2.71}$	$^{+3.87}_{-5.97}$	$^{+1.58}_{-1.76}$	0.96	0.80
1.2 - 1.8	36.46	± 2.74	$^{+7.01}_{-5.80}$	$^{+4.08}_{-5.49}$	$^{+4.38}_{-5.49}$	0.98	0.76
1.8 - 2.8	10.27	± 1.03	$^{+2.91}_{-2.87}$	$^{+0.80}_{-1.44}$	$^{+1.91}_{-2.51}$	0.99	0.71

Table 8: *The differential cross section, $d\sigma/d\Delta\eta_2$, in bins of $\Delta\eta_2$ for "forward jet+dijet" events in the case of $\Delta\eta_1 > 1$. The statistical, systematic and jet-energy-scale uncertainties are shown separately (see the caption of Table 1).*

$(E_{\rm T}^{\rm jet})^2$ (GeV^2)	$\eta^{\rm jet}$ bin	$d^3\sigma/dQ^2d(E_T^{jet})^2d\eta^{\rm jet} \pm \delta_{stat} \pm \delta_{syst}$ (nb/GeV^4)	δ_{CAL}	δ_{FPC}	C_{QED}	C_{HAD}
$20 < Q^2 < 40$ (GeV^2)						
	2.4-2.7	$525 \pm 20^{+61}_{-62}$	$^{+42}_{-63}$	-	0.93	0.88
25-36	2.7-3.1	$658 \pm 24^{+50}_{-44}$	$^{+52}_{-90}$	$^{+1}_{-2}$	0.94	0.91
	3.1-3.7	$463 \pm 20^{+20}_{-31}$	$^{+22}_{-10}$	$^{+66}_{-143}$	0.98	0.86
	3.7-4.3	$359 \pm 13^{+13}_{-18}$	$^{+7}_{-11}$	$^{+111}_{-197}$	0.96	0.93
	2.0-2.4	$133 \pm 4^{+10}_{-10}$	$^{+10}_{-12}$	-	0.96	0.95
	2.4-2.7	$200 \pm 6^{+13}_{-13}$	$^{+15}_{-18}$	-	0.98	0.89
36-100	2.7-3.1	$170 \pm 6^{+6}_{-6}$	$^{+17}_{-14}$	$^{+2}_{-1}$	0.97	0.87
	3.1-3.7	$106 \pm 4^{+6}_{-5}$	$^{+6}_{-7}$	$^{+12}_{-15}$	0.97	0.89
	3.7-4.3	$73.2 \pm 2.6^{+2.6}_{-2.7}$	$^{+1.7}_{-1.2}$	$^{+20.9}_{-27.7}$	1.00	0.88
	2.0-2.4	$17.8 \pm 0.8^{+0.7}_{-0.7}$	$^{+1.2}_{-1.4}$	-	0.99	0.95
	2.4-2.7	$13.3 \pm 0.8^{+0.8}_{-0.7}$	$^{+1.4}_{-1.5}$	-	0.99	0.94
100-400	2.7-3.1	$9.56 \pm 0.68^{+0.42}_{-0.27}$	$^{+0.82}_{-0.95}$	-	0.96	0.92
	3.1-3.7	$6.14 \pm 0.58^{+0.95}_{-0.64}$	$^{+0.41}_{-0.87}$	$^{+0.86}_{-1.55}$	0.97	0.98
	3.7-4.3	$2.66 \pm 0.25^{+0.18}_{-0.16}$	-	$^{+0.83}_{-1.48}$	0.98	0.93
$40 < Q^2 < 100$ (GeV^2)						
	2.4-2.7	$83.6 \pm 5.0^{+3.1}_{-3.2}$	$^{+4.6}_{-7.1}$	$^{+0}_{-0.2}$	0.89	0.90
25-36	2.7-3.1	$105 \pm 5^{+6}_{-4}$	$^{+8}_{-11}$	-	0.94	0.90
	3.1-3.7	$78.3 \pm 4.7^{+4.2}_{-4.2}$	$^{+2.0}_{-4.5}$	$^{+7.8}_{-12.0}$	0.95	0.89
	3.7-4.3	$57.2 \pm 3.0^{+6.1}_{-5.6}$	$^{+0.4}_{-0.9}$	$^{+15.7}_{-26.3}$	0.94	0.85
	2.0-2.4	$24.2 \pm 10.0^{+1.9}_{-1.9}$	$^{+1.5}_{-1.4}$	-	0.94	0.92
	2.4-2.7	$35.8 \pm 1.4^{+2.1}_{-2.2}$	$^{+3.1}_{-2.3}$	-	0.98	0.93
36-100	2.7-3.1	$26.5 \pm 1.2^{+1.5}_{-1.3}$	$^{+2.2}_{-2.2}$	$^{+0.1}_{-0.2}$	0.96	0.88
	3.1-3.7	$19.8 \pm 0.9^{+1.4}_{-1.5}$	$^{+0.9}_{-0.9}$	$^{+1.4}_{-1.5}$	0.96	0.89
	3.7-4.3	$13.7 \pm 0.6^{+0.4}_{-0.4}$	$^{+0.2}_{-0.2}$	$^{+3.1}_{-4.1}$	0.99	0.94
	2.0-2.4	$3.59 \pm 0.18^{+0.21}_{-0.22}$	$^{+0.29}_{-0.30}$	-	0.97	0.97
	2.4-2.7	$2.57 \pm 0.17^{+0.10}_{-0.06}$	$^{+0.17}_{-0.33}$	-	0.96	0.97
100-400	2.7-3.1	$1.71 \pm 0.13^{+0.11}_{-0.19}$	$^{+0.15}_{-0.15}$	-	0.96	0.94
	3.1-3.7	$0.99 \pm 0.08^{+0.16}_{-0.18}$	-	$^{+0.13}_{-0.15}$	0.96	0.96
	3.7-4.3	$0.58 \pm 0.05^{+0.05}_{-0.06}$	-	$^{+0.19}_{-0.30}$	0.97	0.98

Table 9: *The differential cross sections as a function of η^{jet} in different bins of Q^2 and $(E_T^{jet})^2$ for inclusive forward jets. The jet-energy-scale uncertainties are shown separately (see the caption of Table 1).*

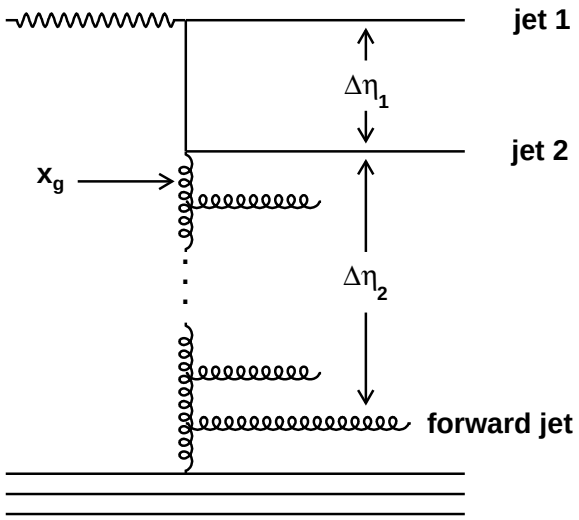

Figure 1: *A schematic diagram of an interaction in which a forward jet and two additional hard jets can be produced.*

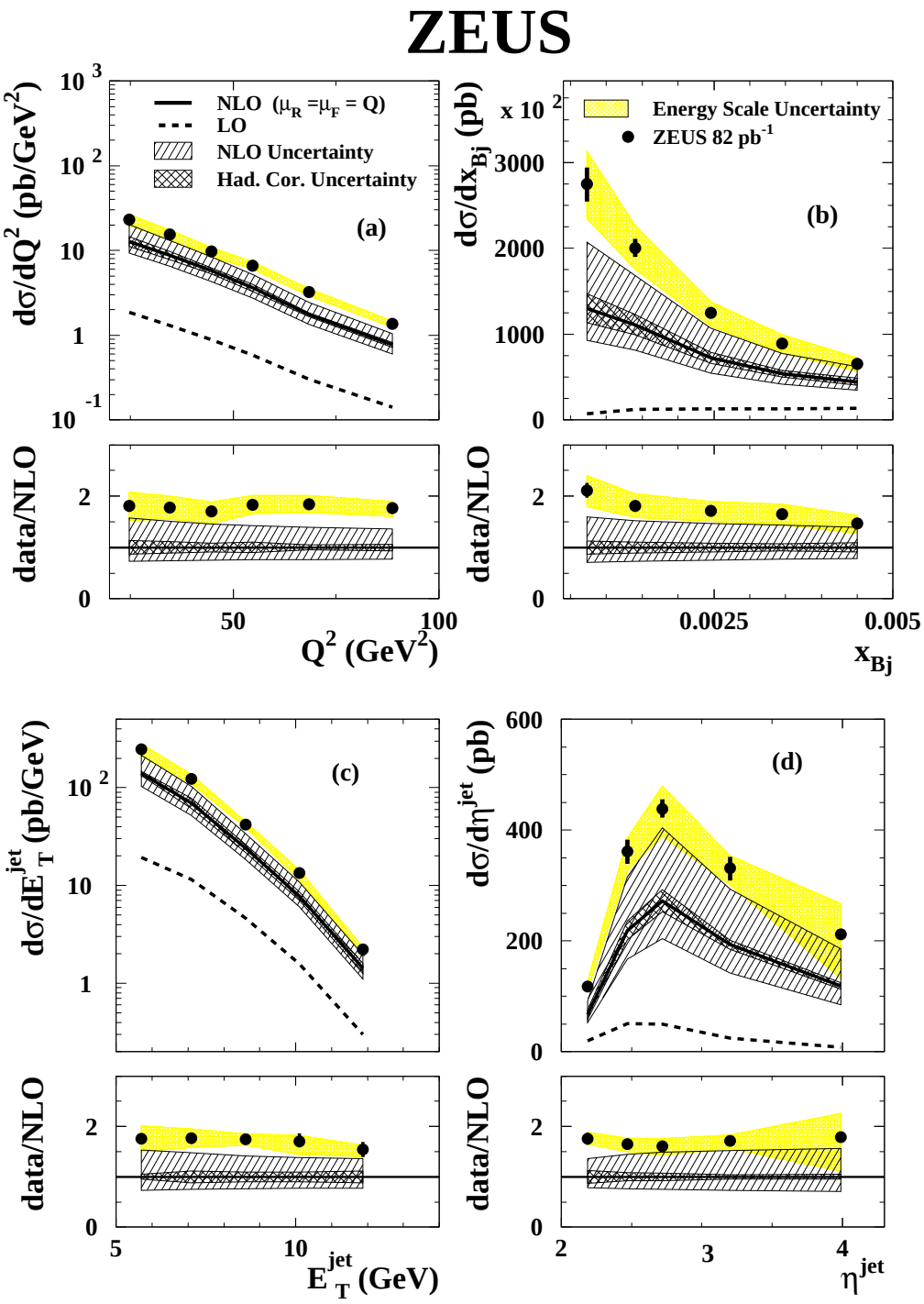

Figure 2: *Measured differential cross sections as a function of (a) Q^2, (b) $x_{\rm Bj}$, (c) E_T^{jet} and (d) η^{jet} for inclusive jet production (dots) compared with the NLO QCD calculations (solid line). The hatched area shows the theoretical uncertainties and the shaded area shows the uncertainty after varying the CAL and FPC energy scales. The inner error bars indicate the statistical uncertainties, while the outer ones correspond to statistical and systematic uncertainties (except the energy-scale uncertainty) added in quadrature.*

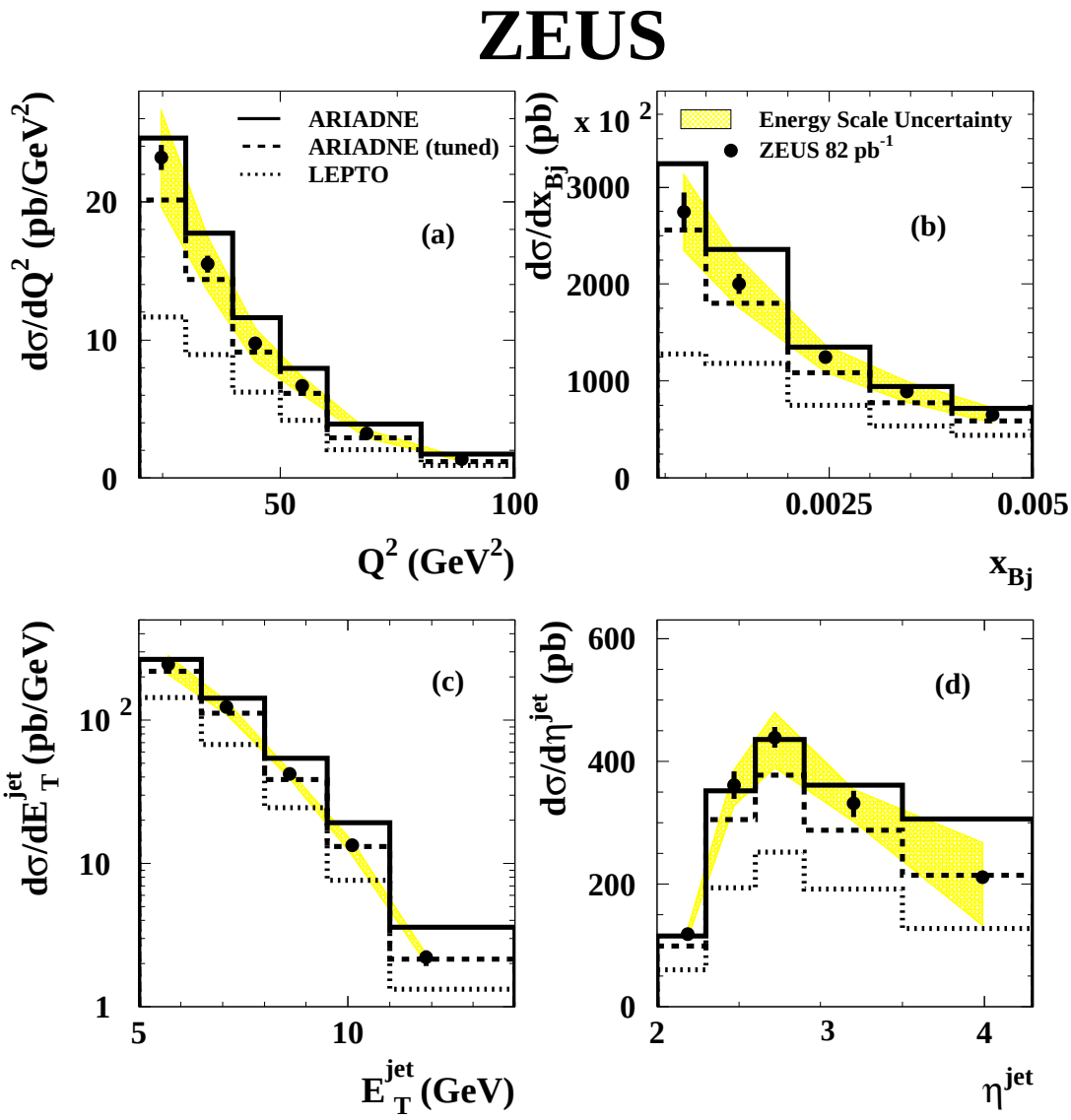

Figure 3: *Measured differential cross sections as a function of (a) Q^2, (b) $x_{\rm Bj}$, (c) E_T^{jet} and (d) η^{jet} for inclusive jet production (dots) compared with the ARIADNE (solid histogram), ARIADNE with new tuning (dashed histogram) and LEPTO (dotted histogram) predictions. The shaded area shows the uncertainty after varying the CAL and FPC energy scales. The inner error bars indicate the statistical uncertainties, while the outer ones correspond to statistical and systematic uncertainties (except the energy-scale uncertainty) added in quadrature.*

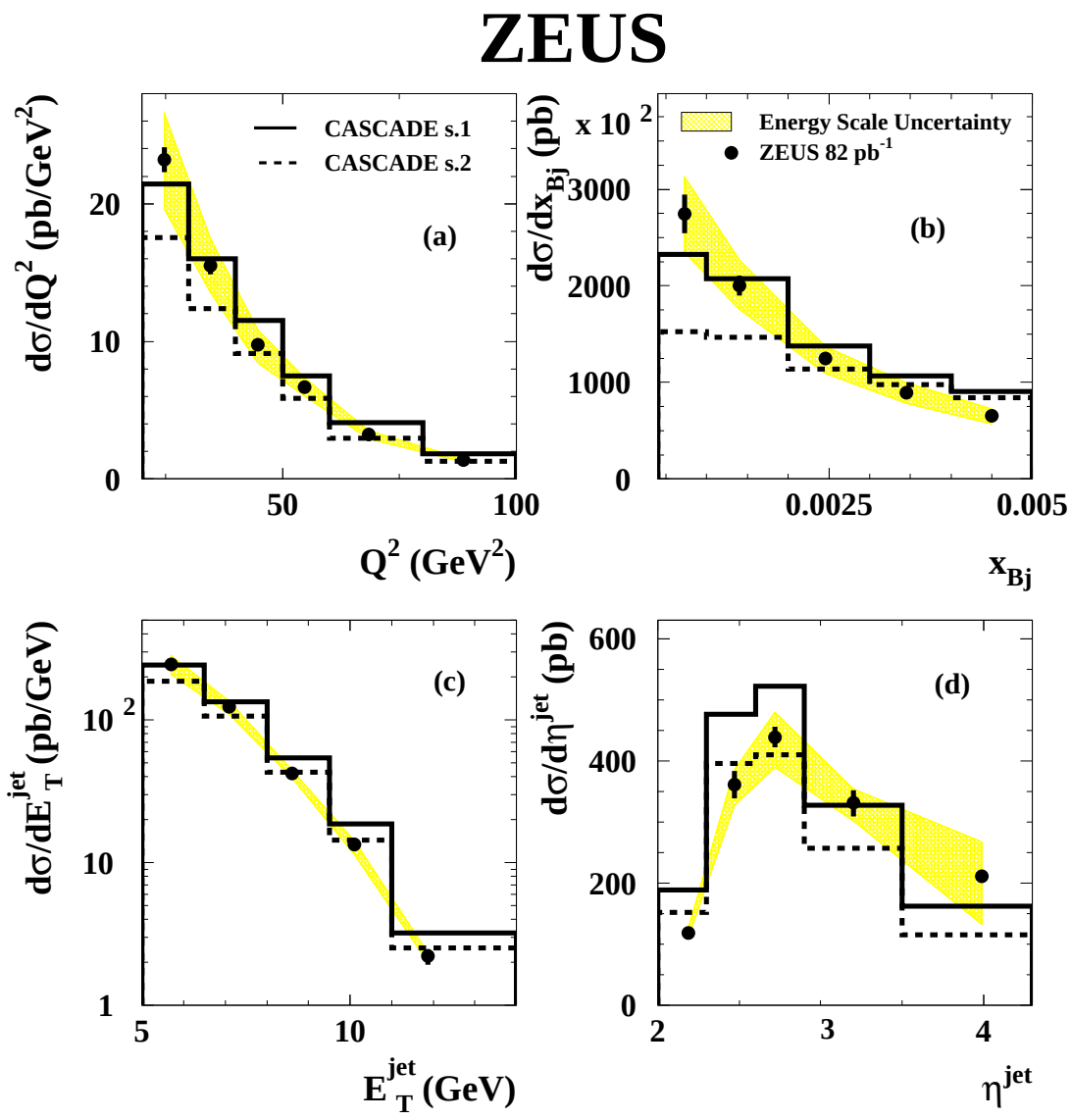

Figure 4: *Measured differential cross sections as a function of (a) Q^2, (b) $x_{\rm Bj}$, (c) E_T^{jet} and (d) η^{jet} for inclusive jet production (dots) compared with the CASCADE set-1 parametrisation (solid histogram) and CASCADE set-2 (dashed histogram) predictions. The shaded area shows the uncertainty after varying the CAL and FPC energy scales. The inner error bars indicate the statistical uncertainties, while the outer ones correspond to statistical and systematic uncertainties (except the energy-scale uncertainty) added in quadrature.*

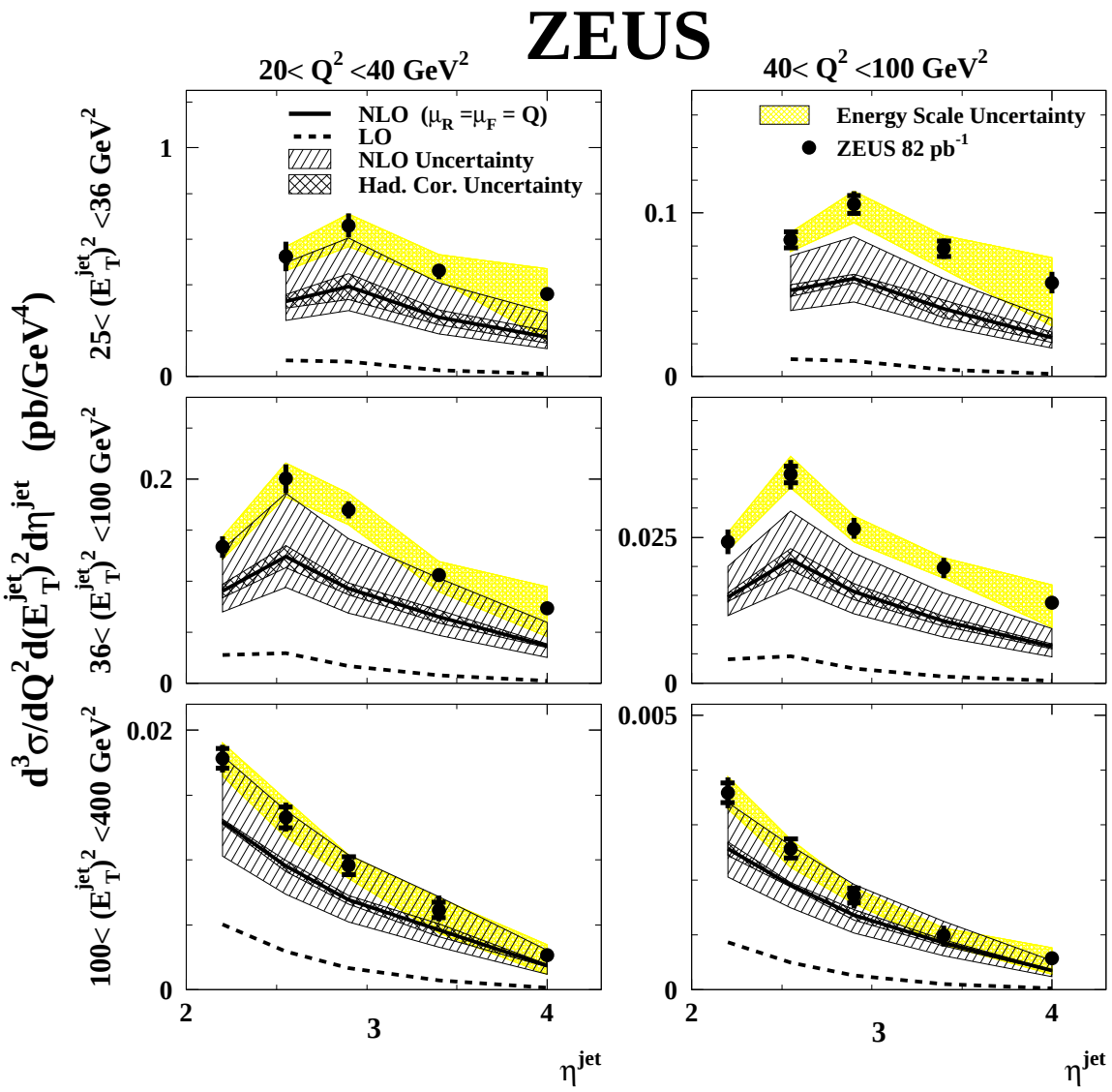

Figure 5: *Measured differential cross sections as a function of η^{jet} in different bins of Q^2 and $(E_T^{jet})^2$ for inclusive jet production (dots) compared with the NLO QCD calculations (solid line). The hatched area shows the theoretical uncertainties and the shaded area shows the uncertainty after varying the CAL and FPC energy scales. The inner error bars indicate the statistical uncertainties, while the outer ones correspond to statistical and systematic uncertainties (except the energy-scale uncertainty) added in quadrature.*

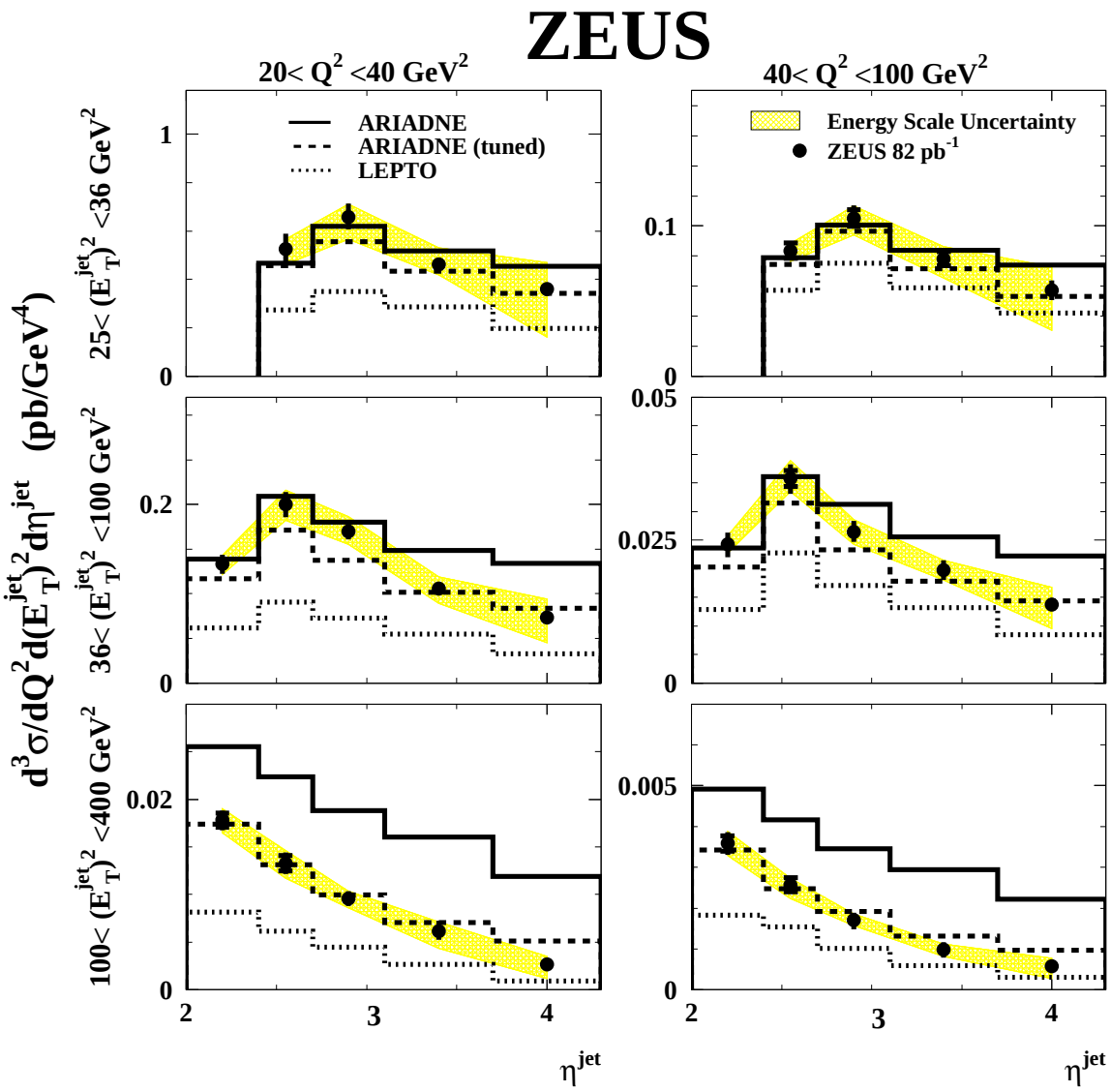

Figure 6: *Measured differential cross sections as a function of η^{jet} in different bins of Q^2 and $(E_T^{jet})^2$ for inclusive jet production (dots) compared with the ARIADNE (solid histogram), ARIADNE with new tuning (dashed histogram) and LEPTO (dotted histogram) predictions. The shaded area shows the uncertainty after varying the CAL and FPC energy scales. The inner error bars indicate the statistical uncertainties, while the outer ones correspond to statistical and systematic uncertainties (except the energy-scale uncertainty) added in quadrature.*

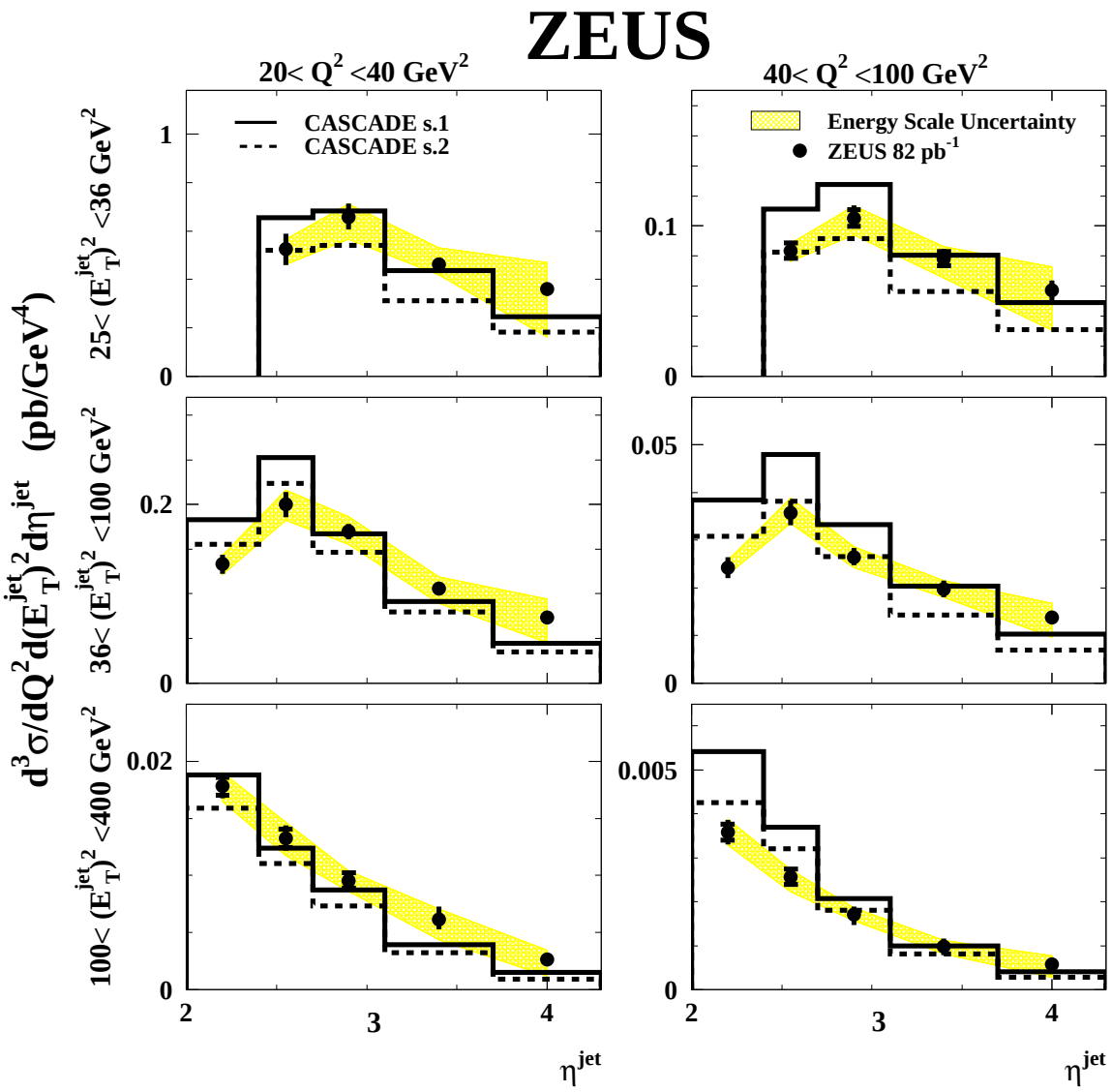

Figure 7: *Measured differential cross sections as a function of η^{jet} in different bins of Q^2 and $(E_T^{jet})^2$ for inclusive jet production (dots) compared with the CASCADE set-1 parametrisation (solid histogram) and CASCADE set-2 (dashed histogram) predictions. The shaded area shows the uncertainty after varying the CAL and FPC energy scales. The inner error bars indicate the statistical uncertainties, while the outer ones correspond to statistical and systematic uncertainties (except the energy-scale uncertainty) added in quadrature.*

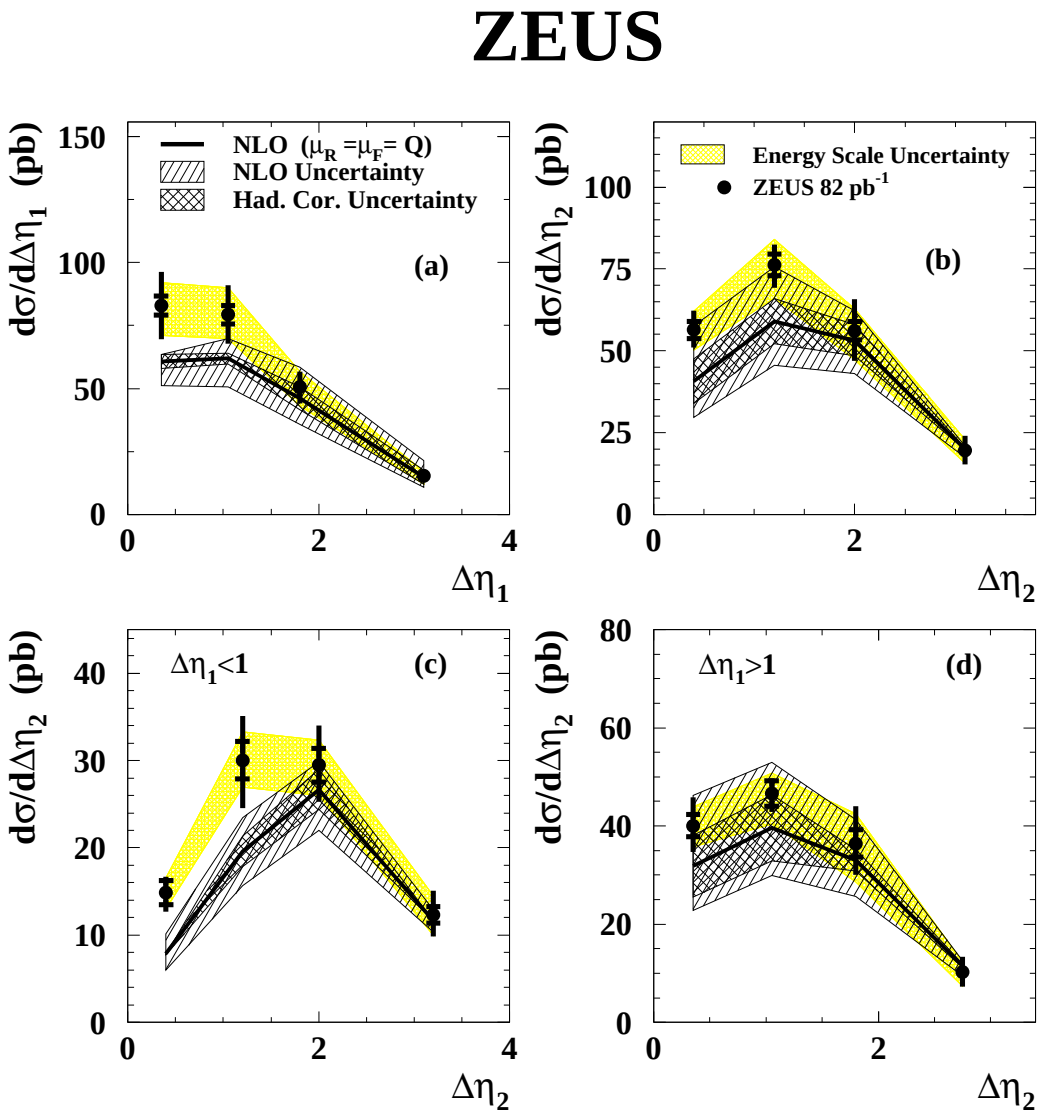

Figure 8: *Differential cross sections for forward+dijet sample as a function of (a) $\Delta\eta_1$, (b) $\Delta\eta_2$, (c) $\Delta\eta_2$ for $\Delta\eta_1 < 1$ and (d) $\Delta\eta_2$ for $\Delta\eta_1 > 1$. The data (dots) are compared with the NLO QCD calculations (solid line). The hatched area shows the theoretical uncertainties. The shaded area shows the uncertainty after varying the CAL and FPC energy scales. The inner error bars indicate the statistical uncertainties, while the outer ones correspond to statistical and systematic uncertainties (except the energy-scale uncertainty) added in quadrature.*

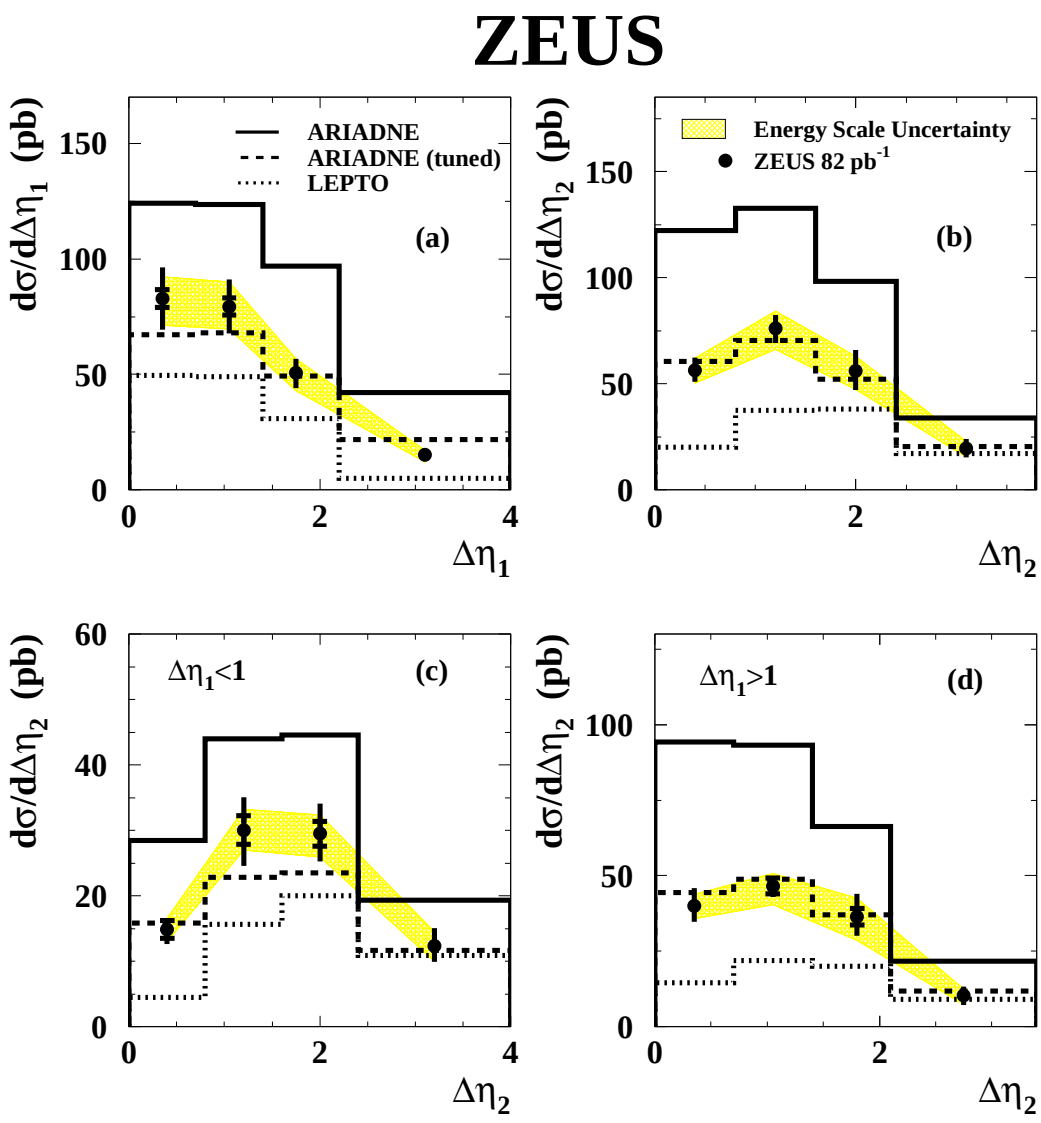

Figure 9: *The differential cross sections for forward+dijet sample as a function of (a) $\Delta\eta_1$, (b) $\Delta\eta_2$, (c) $\Delta\eta_2$, for $\Delta\eta_1 < 1$ and (d) $\Delta\eta_2$ for $\Delta\eta_1 > 1$. The data (dots) are compared with the ARIADNE (solid histogram), ARIADNE with new tuning (dashed histogram) and LEPTO (dotted histogram) predictions. The shaded area shows the uncertainty after varying the CAL and FPC energy scales. The inner error bars indicate the statistical uncertainties, while the outer ones correspond to statistical and systematic uncertainties (except the energy-scale uncertainty) added in quadrature.*

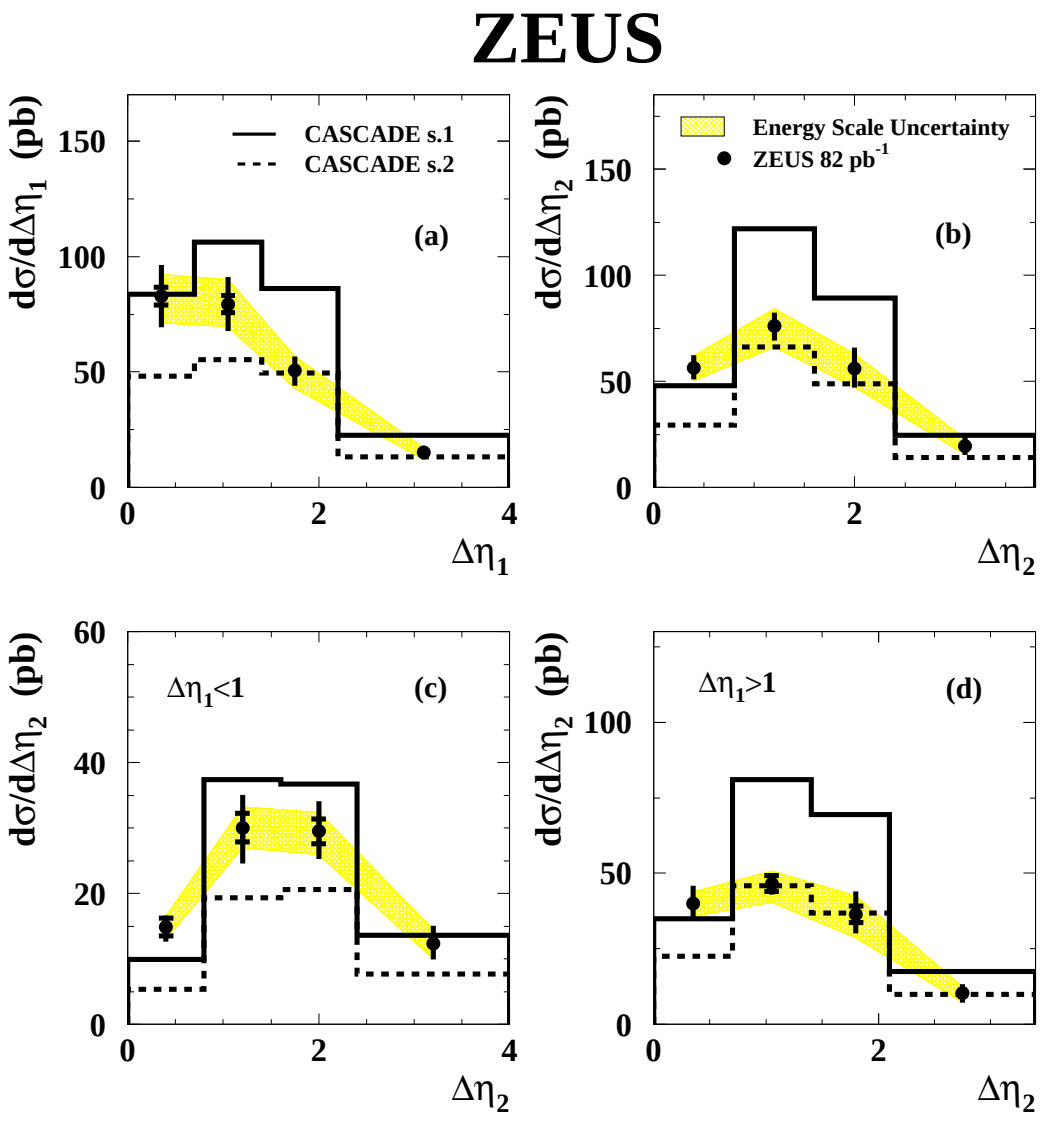

Figure 10: *The differential cross sections for forward+dijet sample as a function of (a) $\Delta\eta_1$, (b) $\Delta\eta_2$, (c) $\Delta\eta_2$, for $\Delta\eta_1 < 1$ and (d) $\Delta\eta_2$ for $\Delta\eta_1 > 1$. The data (dots) are compared with the CASCADE set-1 (solid histogram) and CASCADE set-2 (dashed histograms) predictions. The shaded area shows the uncertainty after varying the CAL and FPC energy scale. The inner error bars indicate the statistical uncertainties, while the outer ones correspond to statistical and systematic uncertainties (except the energy-scale uncertainty) added in quadrature.*